

## Retraction

# Retracted: Acoustic Control through Gradient Coil Design Using a Finite-Difference-Based Method for MRI

### Discrete Dynamics in Nature and Society

Received 23 January 2024; Accepted 23 January 2024; Published 24 January 2024

Copyright © 2024 Discrete Dynamics in Nature and Society. This is an open access article distributed under the Creative Commons Attribution License, which permits unrestricted use, distribution, and reproduction in any medium, provided the original work is properly cited.

This article has been retracted by Hindawi following an investigation undertaken by the publisher [1]. This investigation has uncovered evidence of one or more of the following indicators of systematic manipulation of the publication process:

- (1) Discrepancies in scope
- (2) Discrepancies in the description of the research reported
- (3) Discrepancies between the availability of data and the research described
- (4) Inappropriate citations
- (5) Incoherent, meaningless and/or irrelevant content included in the article
- (6) Manipulated or compromised peer review

The presence of these indicators undermines our confidence in the integrity of the article's content and we cannot, therefore, vouch for its reliability. Please note that this notice is intended solely to alert readers that the content of this article is unreliable. We have not investigated whether authors were aware of or involved in the systematic manipulation of the publication process.

Wiley and Hindawi regrets that the usual quality checks did not identify these issues before publication and have since put additional measures in place to safeguard research integrity.

We wish to credit our own Research Integrity and Research Publishing teams and anonymous and named external researchers and research integrity experts for contributing to this investigation.

The corresponding author, as the representative of all authors, has been given the opportunity to register their agreement or disagreement to this retraction. We have kept a record of any response received.

### References

- [1] L. Kang and L. Xia, "Acoustic Control through Gradient Coil Design Using a Finite-Difference-Based Method for MRI," *Discrete Dynamics in Nature and Society*, vol. 2021, Article ID 3719618, 8 pages, 2021.

## Research Article

# Acoustic Control through Gradient Coil Design Using a Finite-Difference-Based Method for MRI

Liyi Kang <sup>1</sup> and Ling Xia <sup>1,2</sup>

<sup>1</sup>Department of Biomedical Engineering, Zhejiang University, Hangzhou 310027, China

<sup>2</sup>State Key Lab of CAD and CG, Zhejiang University, Hangzhou 310027, China

Correspondence should be addressed to Liyi Kang; 05swyxkly@zju.edu.cn

Received 22 August 2021; Revised 25 September 2021; Accepted 18 October 2021; Published 31 October 2021

Academic Editor: Ahmed Farouk

Copyright © 2021 Liyi Kang and Ling Xia. This is an open access article distributed under the Creative Commons Attribution License, which permits unrestricted use, distribution, and reproduction in any medium, provided the original work is properly cited.

An acoustic control scheme is proposed in this paper through the process of gradient coil design for magnetic resonance imaging (MRI). With a finite-difference-based method, the stream function and coil displacement caused by fast gradient switching can be unified by a simplified momentum equation, which can be incorporated into the conventional gradient coil design. A three-dimensional transverse gradient coil with an edge-connected cylindrical structure is used as a design example to verify the proposed design method. In addition, an acoustic model is established to simulate the sound pressure level (SPL). In the model, two hemispherical air volumes are added flush with the ends of the cylindrical main magnet to mimic the free propagation of sound waves on the boundaries. The simulation results show that by optimizing coil displacement, the overall SPL can be attenuated by 4 dB over the frequency range from 0 to 3000 Hz with the displacement reduced by about 50%, at the cost of a figure of merit (FOM) loss by about 8%. Therefore, the proposed acoustic control scheme can be used as a complement to conventional acoustic control methods for further noise reduction.

## 1. Introduction

During MRI scanning, significant Lorentz forces are produced by fast gradient switching, which leads to vibration of the gradient assembly and induces loud acoustic noise inside the patient bore [1, 2]. The sound pressure level (SPL) of this acoustic noise can reach 130 dB in some MRI scanners [3]. This serious noise may not only cause patient discomfort and affect image quality but also damage the patient's auditory system. Therefore, acoustic noise control has become an important issue in MRI system design.

To mitigate the effect of acoustic noise, some engineers and scholars attempted to block the noise propagation. A simple and frequently used scheme is to isolate the patient's auditory system, such as wearing earplugs or helmet [4]. Adding an appropriately designed passive acoustic liner into the gradient assembly can be another scheme to significantly reduce the noise level [5]. It is also reported that sealing the gradient coil in a vacuum chamber [6, 7] or

using damping materials [8, 9] can be feasible methods for noise control.

In addition to blocking the noise propagation, attenuating noise level from the noise source is another scheme of noise elimination. One method of this category is active noise control [10–14], which generates active acoustic noise with equal amplitude and opposite phase to counteract the original noise. However, the results showed that this method was mainly effective at low frequency due to its low modal density and long wavelength. Considering the positive correlation between acoustic noise and gradient pulse, Hennel et al. proposed soft gradient pulses, using sinusoidal components to replace linear varying gradient pulse and reduce noise level [15, 16]. Although this method was efficient, different pulse shapes may degrade the image quality.

In order to further eliminate acoustic noise in MRI systems, numerous mathematical models were proposed in past decades to quantitatively investigate the generation and propagation of acoustic noise. Shao et al. used analytical

methods for noise analysis in cylindrical ducts [17, 18]. Based on this method, Forbes et al. proposed an analytical gradient coil design method to control acoustic noise [19, 20]. Though their analytical method was efficient in computation, it was restricted to specific cylindrical coil structure. Numerical methods in acoustic noise modelling also developed rapidly. Statistical energy analysis [7] was used as a numerical method to analyze acoustic noise in the early years. With the development of computational performance, the finite element method (FEM) and boundary element method (BEM) have become increasingly used for noise numerical analysis [21–25]. To accurately simulate acoustic noise, Lorentz damping was also considered in noise modelling by Winkler et al. Their study indicated that the simulated results using their model showed a general agreement to the experimental data [26].

These models have laid the foundation for acoustic analysis of MRI system and provided useful tools for MRI noise control. However, attenuating acoustic noise through the coil design process based on numerical method has not been fully explored. In this paper, a finite-difference-based numerical gradient coil design method is proposed for acoustic noise reduction through optimizing coil displacement caused by Lorentz force. Different from most noise control methods, the proposed method does not need to add extra parts to MRI apparatus. An edge-connected three-dimensional (3D) cylindrical gradient coil structure is used as a design example. Design results of the gradient coil in the same structure without a noise control scheme are also presented for comparison.

## 2. Method

**2.1. Coil Configuration.** An edge-connected cylindrical transverse gradient coil is chosen to be the design example for acoustic control in this paper, as shown in Figure 1. Gradient coil is distributed on the cylindrical surfaces including three parts: the primary layer closest to the region of interest (ROI) where the generated gradient field should be highly linear; the shielding layer covering the primary layer, on which the coil produces a reverse magnetic field to counteract the stray field on the shielding region; and the connecting part between the primary and shielding layers. The ROI is an oblate spheroid with a length of 50 cm in  $x$  and  $y$  directions and 40 cm in  $z$ -direction. The diameters of the inner and outer cylindrical walls  $D_1$  and  $D_2$  are 68.8 cm and 87 cm, respectively, while the length of the inner wall  $L_1$  is 86.8 cm and  $L_2 = 111$  cm.

**2.2. Matrix Equation for Finite-Difference-Based Gradient Coil Design.** A volumetric finite-difference method (FDM) was recently proposed for complex-structured gradient coil design [27]. Due to its simplicity and flexibility, this method is applied in this paper and extended for acoustic noise control. Using this method to design gradient coil, the coil space where current density  $J$  is distributed needs to be discretized by a group of gridlines along mutually orthogonal directions  $p$  and  $q$ .

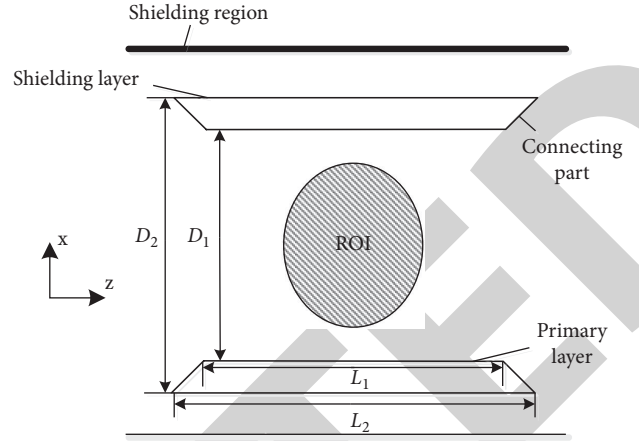


FIGURE 1: The cross section of the edge-connected cylindrical gradient coil. Gradient coil is distributed on the cylindrical surfaces including the primary layer, the shielding layer, and the connecting part.

Numerous quasi-rectangular elements are in this way formed on the coil space surface. In the design of this paper, these gridlines are chosen to be along the direction of cylindrical coordinates. Suppose vector  $n$  points to the normal direction of the element surface; Figure 2 illustrates a single discretized element in a local coordinate system  $(p, q, n)$ .

In the gradient coil design, the stream function  $\varphi$  defined as the vector potential of current density should be determined, as the contour lines of the stream function indicate the location of wires [28]. According to the definition of the vector potential, the current density can be expressed as a first-order finite-difference form in the local coordinate system  $(p, q, n)$ :

$$J_p(i, j + 0.5) \approx \frac{\Delta\varphi_q(i, j)}{\Delta q_{i,j}} = \frac{\varphi(i, j + 1) - \varphi(i, j)}{\Delta q_{i,j}},$$

$$J_q(i + 0.5, j) \approx -\frac{\Delta\varphi_p(i, j)}{\Delta p_{i,j}} = -\frac{\varphi(i + 1, j) - \varphi(i, j)}{\Delta p_{i,j}}. \quad (1)$$

To unify the current density from different elements in a global Cartesian coordinate system, a transformation of coordinates is then used:

$$J_x^{(c)} = J_p^{(c)} \frac{\Delta x_{i,j+0.5}}{\Delta p_{i,j+0.5}} + J_q^{(c)} \frac{\Delta x_{i+0.5,j}}{\Delta q_{i+0.5,j}},$$

$$J_y^{(c)} = J_p^{(c)} \frac{\Delta y_{i,j+0.5}}{\Delta p_{i,j+0.5}} + J_q^{(c)} \frac{\Delta y_{i+0.5,j}}{\Delta q_{i+0.5,j}}, \quad (2)$$

$$J_z^{(c)} = J_p^{(c)} \frac{\Delta z_{i,j+0.5}}{\Delta p_{i,j+0.5}} + J_q^{(c)} \frac{\Delta z_{i+0.5,j}}{\Delta q_{i+0.5,j}},$$

in which  $x$ ,  $y$ , and  $z$  are three directions of the global Cartesian coordinate and  $(c)$  denotes the centre point of an element. According to the Biot–Savart law, the  $z$  component of magnetic flux density  $B_z$  generated by an element on coil space can be calculated approximately as follows:

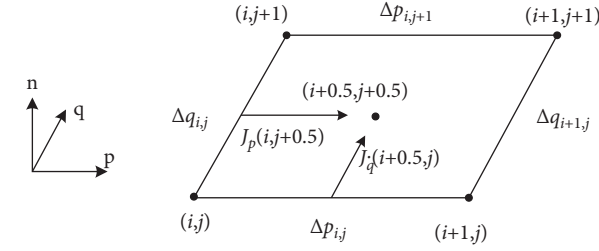


FIGURE 2: The discretized quasi-rectangular element and nodes in a local coordinate system  $(p, q, n)$ .  $J_p$  and  $J_q$  denote the directions of current density;  $(i, j)$  indicates the index of corresponding node.

$$B_z = \frac{\mu_0}{4\pi} \frac{J_x^{(c)}(y_f - y_c) - J_y^{(c)}(x_f - x_c)}{|R^{(c)}|^3} S, \quad (3)$$

where  $S$  is the area of the grid element and  $\mathbf{R}^{(c)}$  is the vector pointing from the centre point of the selected element to a specific field point  $(x_f, y_f, z_f)$ . Therefore, a matrix equation can be established by combining equations (1)–(3) to describe the relationship between the stream function  $\varphi$  and generated magnetic flux density  $\mathbf{B}$  over a specific field point region:

$$\mathbf{A}\varphi = \mathbf{B}, \quad (4)$$

where  $\mathbf{A}$  is a sensitivity coefficient matrix. In the design, the field point region includes the ROI and the shielding region.

**2.3. Lorentz Force and Coil Displacement.** Suppose the deformation material is elastically isotropic; the momentum equation for this linearized elastodynamic problem is given by [29]

$$\rho_M \frac{\partial^2 \mathbf{u}}{\partial t^2} = \rho_M \mathbf{f}_i + \sum_{j=1}^3 \frac{\partial \sigma_{ji}}{\partial x_j}, \quad i = 1, 2, 3, \quad (5)$$

in which  $\mathbf{u}$  and  $\mathbf{f}$  are the displacement and body force vectors, respectively;  $\rho_M$  is the density of the isotropic material;  $i$  and  $j$  indicate three orthogonal directions; and  $\sigma$  represents the component of the stress tensor in the corresponding direction. In the design, the body force  $\mathbf{f}$  comes from the Lorentz force caused by gradient switching and can be calculated by Lorentz force law:

$$\mathbf{f}_i = \frac{1}{\rho_M w} (\mathbf{j} \times \mathbf{B}), \quad (6)$$

where  $w$  is the thickness of the conductor layer. In addition, the nine components of the stress tensor are related to the components of the strain tensor satisfying [30]

$$\sum_{i,j=1}^3 \frac{\partial \sigma_{ji}}{\partial x_j} = (\Lambda + G) \nabla (\nabla \cdot \mathbf{u}) + G \nabla^2 \mathbf{u}, \quad (7)$$

in which

$$G = \frac{E}{2(1+\nu)}, \quad (8)$$

$$\Lambda = \frac{\nu E}{(1+\nu)(1-2\nu)},$$

where  $E$  and  $\nu$  are Young's modulus and the Poisson ratio, respectively. Obviously, only the normal component  $u_n$  of the displacement vector is needed to be considered, since this component perpendicular to the coil surface will be the main cause to propel the air inside the patient bore and produce acoustic noise. In addition, the first term on the right side of equation (7) can also be ignored, as the variation of  $u_n$  along the normal direction is approximately zero ( $\partial u_n / \partial n = 0$ ). Therefore, equation (5) becomes

$$\rho_M \frac{\partial^2 u_n}{\partial t^2} = \frac{1}{w} (j_p B_q - j_q B_p) + G \nabla^2 u_n, \quad (9)$$

where  $B_p$  and  $B_q$  are  $\mathbf{p}$ ,  $\mathbf{q}$  components of the strong static magnetic field, which can be derived with a transformation of coordinates.

To further simplify equation (9), we assumed the response of the Lorentz force to gradient change and the deformation to Lorentz force are completed instantaneously, and all these variables follow the time-dependent behaviour:

$$j_p = f(t) \tilde{j}_p, \quad j_q = f(t) \tilde{j}_q, \quad u_n = f(t) \tilde{u}_n, \quad (10)$$

where  $f(t)$  is a function representing gradient switching with amplitude 1. We set  $f(t)$  to be the sinusoidal function with angular frequency  $\omega$  in this paper. Therefore, equation (9) can be simplified as follows:

$$-\rho_M \omega^2 \tilde{u}_n = \frac{1}{w} (\tilde{j}_p B_q - \tilde{j}_q B_p) + G \nabla^2 \tilde{u}_n. \quad (11)$$

As shown in Figure 3, the second-order finite-difference scheme is applied to a quasi-rectangular unit formed by four small grid elements, which gives

$$\begin{aligned} \nabla^2 \tilde{u}_n &= \frac{\partial^2 \tilde{u}_n}{\partial p^2} + \frac{\partial^2 \tilde{u}_n}{\partial q^2} \\ &\approx \frac{\tilde{u}_n(i-1, j) - \tilde{u}_n(i, j) + \tilde{u}_n(i+1, j)}{\Delta p^2} + \frac{\tilde{u}_n(i, j-1) - \tilde{u}_n(i, j) + \tilde{u}_n(i, j+1)}{\Delta q^2}. \end{aligned} \quad (12)$$

Applying equations (11) and (12) to the whole coil space surface, the following matrix equations can be obtained:

$$\begin{aligned} M_\varphi \varphi &= M_u \tilde{u}_n \Rightarrow \tilde{u}_n = M_u^{-1} M_\varphi \varphi \\ \tilde{u}_n^2 &= \varphi^T \left[ M_\varphi^T (M_u^{-1})^T M_u^{-1} M_\varphi \right] \varphi = \varphi^T L_d \varphi. \end{aligned} \quad (13)$$

**2.4. Optimization Problem.** In the previous sections, the coefficient matrices to calculate coil displacement and generated magnetic field using stream function value were obtained. In addition to these parameters, dissipated power is also a frequently used target for optimization in gradient coil design. Similarly, dissipated power produced by gradient coil can be conveniently written with a finite-difference-based equation. According to the definition, dissipated power  $P_d$  can be calculated as follows:

$$P_d = \iint_{R_p, R_q} (J_p^2 + J_q^2) dpdq. \quad (14)$$

Substituting finite-difference scheme equation (1) into equation (14), the following matrix equation is obtained:

$$P_d = \varphi^T L_p \varphi. \quad (15)$$

Considering all these parameters, the following optimization problem is established to design an optimized gradient coil:

$$\begin{aligned} \min \quad & \varphi^T (L_p + \lambda L_d) \varphi \\ \text{subject to} \quad & \\ \max \quad & |A_1 \varphi - B_{z, \text{ideal}}| < \varepsilon_1 \max \Delta B_z, \\ \max \quad & |A_2 \varphi| < \varepsilon_2 \max B_{\text{stray}} \end{aligned} \quad (16)$$

where  $A_1$  and  $A_2$  are coefficient matrices to calculate generated magnetic field over ROI and the stray region, respectively;  $\lambda$  is a weighting coefficient; and  $\varepsilon_1$  and  $\varepsilon_2$  are parameters selected according to the design requirement. This optimization problem was solved by the function *quad* from the software MATLAB (MathWorks, Natick, MA, USA).

**2.5. Acoustic Modelling and Simulation.** Based on the designed gradient coil, an acoustic model shown in Figure 4 was constructed for the evaluation of noise level. The

gradient coil was embedded in the epoxy (Young's modulus  $E$ : 10 GPa, Poisson ratio  $\nu$ : 0.4, and density: 1600 kg/m<sup>3</sup>) and placed into the cylindrical bore duct formed by the main magnet (diameter: 1.2 m) modelled with sound hard boundary. The air (speed of sound: 343 m/s; density: 1.2 kg/m<sup>3</sup>) inside the bore was governed by the sound wave propagation equation [19]. The air volume of two hemispheres (radius: 1.2 m) flush with the cylinder end was added to the model to mimic the infinite simulation domain. The sound wave was allowed to freely propagate outwards through the perfectly matched layer without reflection. The simulation was implemented by a harmonic study with a frequency range from 0 Hz to 3000 Hz (step size: 50 Hz), covering the frequency range of most MRI pulse sequences. The multi-physics package COMSOL (COMSOL Inc., Burlington, MA, USA) was used for modelling and simulation in this work.

### 3. Results and Discussion

In this section, the design results obtained by solving the optimization problem (16) are shown to validate the effectiveness of the proposed method in reducing coil displacement and controlling noise levels. The design parameters  $\varepsilon_1$  and  $\varepsilon_2$  were chosen to be 0.05 and 0.03, respectively, which were frequently used values in gradient coil design. The thickness of the epoxy layer  $w$  is equal to 5 mm, and the frequency of the sinusoidal gradient pulse was set to be 1750 Hz in equation (11), which is near the root mean square (RMS) of the frequency range 0 to 3000 Hz, to find an optimized solution over the whole frequency range.

In order to describe coil performance, several parameters are chosen in this paper, including max field deviation  $\Delta B_z^{\max}$ , gradient efficiency  $\eta$ , and figure of merit (FOM). These parameters are defined by

$$\begin{aligned} \Delta B_z^{\max} &= \max \left( \frac{|B_{T,z} - B_{\text{ideal},z}|}{\max |B_{T,z}|} \right), \\ \eta &= \frac{G_0}{I}, \\ \text{FOM} &= \frac{\eta^2}{L}, \end{aligned} \quad (17)$$

where  $B_{T,z}$  and  $B_{\text{ideal},z}$  are the generated and ideal magnetic fields within ROI, respectively;  $G_0$  indicates the gradient

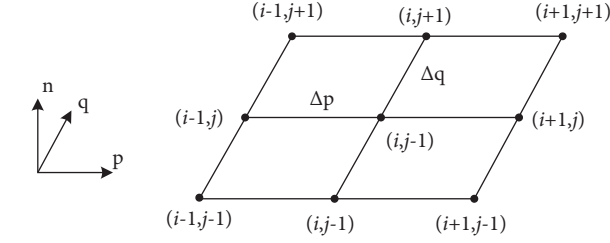


FIGURE 3: A quasi-rectangular unit formed by four grid elements for applying second-order finite-difference scheme.

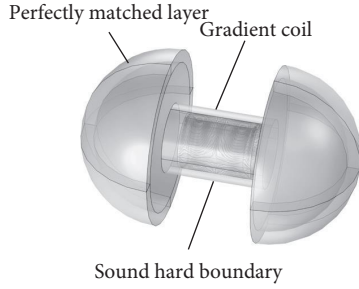


FIGURE 4: The constructed model for the evaluation of noise level. The gradient coil was surrounded by a cylindrical surface modelled with sound hard boundary. Two hemispheres flush with the cylinder end were added to model perfectly matched layers.

strength at the centre point of ROI; and  $I$  is the transport current, while  $L$  denotes coil inductance calculated by software FastHenry [31]. The transport current  $I$  can be calculated as follows:

$$I = \frac{\max \varphi - \min \varphi}{N_t}, \quad (18)$$

where  $N_t$  denotes the winding turns. In these parameters, max field deviation is used to describe the field linearity; FOM is very useful to evaluate coil inductance characteristics, as they are independent of the winding turns.

**3.1. Coil Winding and Performances.** Figure 5 shows the winding patterns of the designed gradient coil, and the coil performance is listed in Table 1. The performance of a conventional coil with the same structure without displacement control is also included in Table 1 for comparison, designed by specifying  $\lambda = 0$  in optimization problem (16).

It can be seen in Table 1 that the optimized coil and conventional coil have similar transport current, gradient efficiency, and minimum wire gap. Since the max field deviation and  $\max(B_z^{\text{stray}})/\max(B_z^{\text{dsv}})$  can be controlled in the design process by adjusting  $\varepsilon_1$  and  $\varepsilon_2$ , these values of the two coils are equivalent. The major difference lies in their displacements, FOM, and inductance and resistance values. Compared to the conventional coil without displacement control, the displacement (RMS) of the optimized coil at 1750 Hz is significantly reduced (about 43%) at the cost of about 8% FOM. Though the FOM is slightly reduced, it is still greater than that of the most frequently used 2D cylindrical gradient coils without the connecting layer (FOM is usually less than  $5 \mu\text{T}^2 \cdot \text{m}^{-2} \cdot \text{A}^{-2} \cdot \text{H}^{-1}$  in this case). Therefore,

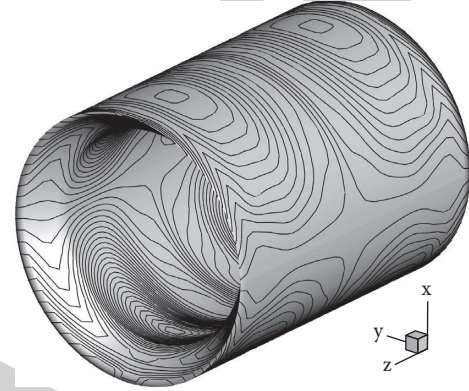


FIGURE 5: Winding patterns of the designed cylindrical transverse gradient coil with displacement optimization. The transport current is 439.1 A for the target gradient strength of 30 mT/m, and the minimum wire gap is 3.9 mm.

TABLE 1: Characteristics of the designed coils.

Coil property	Optimized coil	Conventional coil
Transport current (A)	439.1	447.0
Efficiency ( $\mu\text{T} \cdot \text{m}^{-1} \cdot \text{A}^{-1}$ )	67.91	66.74
Max field deviation, $\Delta B_z^{\text{max}}$ (%)	5.0	5.0
Max ( $B_z^{\text{stray}}/\max(B_z^{\text{dsv}})$ ) (%)	3.0	3.0
Min. wire gap (mm)	3.9	4.2
Inductance ( $\mu\text{H}$ )	647	574
Resistance (m $\Omega$ )	474	429
Displacement (RMS), $f = 1750 \text{ Hz}(\mu\text{m})$	1.2	2.1
FOM <sub>1</sub> , $\eta^2/L$ ( $\mu\text{T}^2 \cdot \text{m}^{-2} \cdot \text{A}^{-2} \cdot \text{H}^{-1}$ )	7.13	7.76

the optimized coil still has satisfactory electromagnetic property with reduced displacement caused by Lorentz force.

**3.2. Displacement and SPL at Different Frequencies.** The displacement reduction shows an improvement of displacement control at a specific frequency (1750 Hz) when compared to the existing method [25]. In this section, the displacement and average SPLs at different frequencies will be discussed.

Figure 6 shows the displacement and SPL over the frequency range from 0 to 3000 Hz for the designed optimized and conventional gradient coils. For the conventional

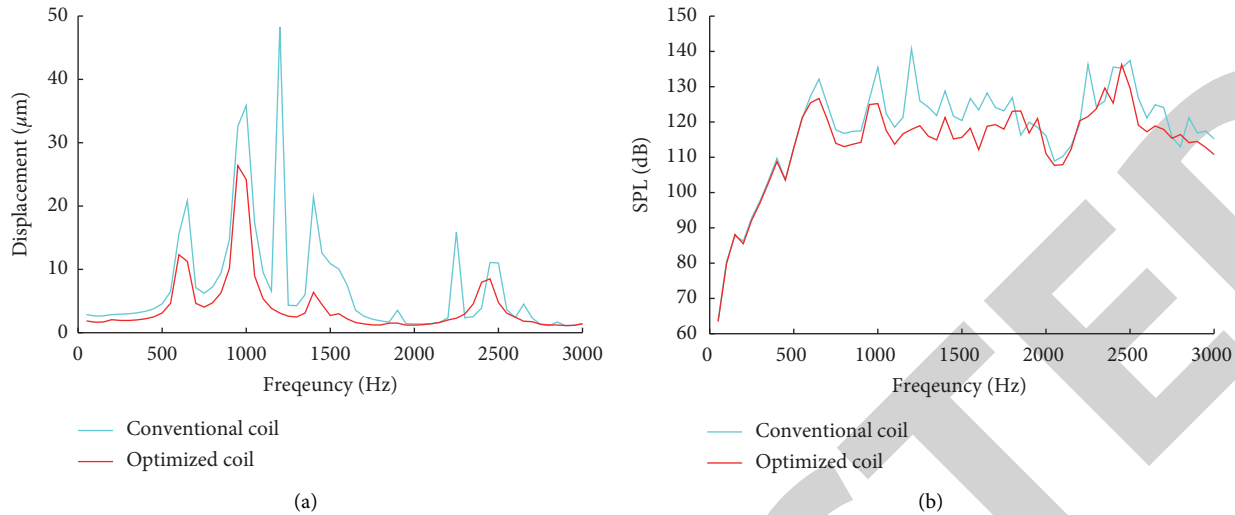


FIGURE 6: The (a) displacement of gradient coils and (b) corresponding average SPL in the patient bore over the frequency range from 0 to 3000 Hz.

coil without displacement optimization, the maximum displacement and SPL are reached at the frequency of 1200 Hz with the value of about 48  $\mu\text{m}$  and 141 dB; however, for the case of the optimized coil, the maximum displacement is about 26  $\mu\text{m}$  at the frequency of 950 Hz, while the maximum SPL is about 136 dB at 2450 Hz. One possible reason for this variation is that coil has its own natural frequency and behaves in different modes when responding to the gradient pulse with the same frequency.

Although two gradient coils respond in different modes, the overall displacement and SPL are reduced after displacement optimization. It can be calculated from the simulation results that the RMS of displacement and SPL over the frequency range are reduced from 12  $\mu\text{m}$ , 119 dB, to 6  $\mu\text{m}$ , 115 dB, respectively. This result implies that the acoustic noise level can be attenuated by optimizing displacement. Figure 7 illustrates that the displacement ratio and SPL difference of the conventional and optimized gradient coils are generally consistent over the frequency range.

From the coil design process, we can see that it is very convenient to incorporate the momentum equation describing the relationship between Lorentz force and displacement into the gradient coil design by using the finite-difference method. Compared to other numerical gradient coil design methods, such as FEM and BEM, the finite-difference method provides a straightforward scheme to deal with second-order differential terms in the momentum equation. In addition, the quasi-rectangular mesh structure discretized with gridlines along cylindrical coordinate directions is more simple than the triangular elements used in FEM and BEM, which require extra computational effort.

Although the SPL over the frequency range is only reduced by 4 dB in the design example, acoustic control through gradient coil design is still of a certain value. Compared with other frequently used methods, the impact on the other parts of the MRI apparatus is very small when using an optimized gradient coil, meaning that it is feasible to combine the

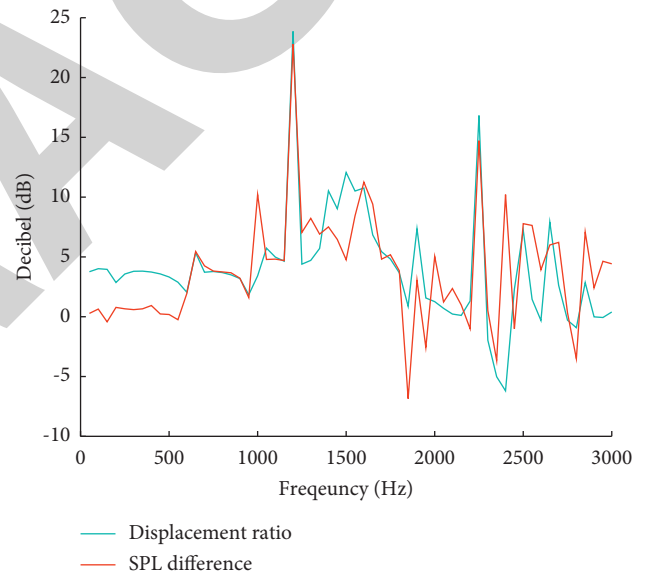


FIGURE 7: Comparison between the displacement ratio and SPL difference of the conventional and optimized gradient coils over the frequency range from 0 to 3000 Hz.

optimized coil with other methods to further attenuate acoustic noise. Moreover, different gradient assemblies can be designed for specific pulse sequences with different frequency characteristics for better acoustic control. Therefore, the proposed optimized gradient coil can be used as a complement to contemporary acoustic control methods.

#### 4. Conclusion

In this paper, a finite-difference-based gradient coil design method is proposed for acoustic noise control. The new method attempts to reduce noise levels through coil displacement optimization in the coil design process. By applying the first-order and second-order finite-difference

schemes, matrix equations are constructed and an optimization problem is established, which is used to solve for gradient coil data. In addition, modelling for calculating displacement and SPL over a frequency range from 0 to 3000 Hz is also included in the work. The simulation results show that the optimized coil produces less displacement and SPL. Compared to other noise control measures, the proposed method does not need to add extra parts to the MRI apparatus. Therefore, this easy-to-implement method can be used as a complement for further noise reduction.

## Data Availability

The data used to support the findings of this study are included within this article.

## Conflicts of Interest

The authors declare that they have no conflicts of interest.

## References

- [1] S. A. Counter, A. Olofsson, H. F. Grahn, and E. Borg, "MRI acoustic noise: sound pressure and frequency analysis," *Journal of Magnetic Resonance Imaging*, vol. 7, no. 3, pp. 606–611, 1997.
- [2] J. P. McNulty and S. McNulty, "Acoustic noise in magnetic resonance imaging: an ongoing issue," *Radiography*, vol. 15, no. 4, pp. 320–326, 2009.
- [3] M. E. Ravicz, J. R. Melcher, and N. Y.-S. Kiang, "Acoustic noise during functional magnetic resonance imaging," *Journal of the Acoustical Society of America*, vol. 108, no. 4, pp. 1683–1696, 2000.
- [4] M. E. Ravicz and J. R. Melcher, "Isolating the auditory system from acoustic noise during functional magnetic resonance imaging: examination of noise conduction through the ear canal, head, and body," *Journal of the Acoustical Society of America*, vol. 109, no. 1, pp. 216–231, 2001.
- [5] C. Mechefske, R. Geris, J. S. Gati, and B. K. Rutt, "Acoustic noise reduction in a 4T MRI scanner," *Magnetic Resonance Materials in Biology, Physics, and Medicine*, vol. 13, no. 3, pp. 172–176, 2002.
- [6] A. Katsunuma, H. Takamori, Y. Sakakura, Y. Hamamura, Y. Ogo, and R. Katayama, "Quiet MRI with novel acoustic noise reduction," *Magnetic Resonance Materials in Biology, Physics, and Medicine*, vol. 13, no. 3, pp. 139–144, 2002.
- [7] W. A. Edelstein, R. A. Hedeem, R. P. Mallozzi, S.-A. El-Hamamsy, R. A. Ackermann, and T. J. Havens, "Making MRI quieter," *Magnetic Resonance Imaging*, vol. 20, no. 2, pp. 155–163, 2002.
- [8] H. Takamori, A. Katsunuma, Y. Uosaki, T. Toyoshima, K. Iinuma, and H. Kawamoto, "Magnetic resonance imaging system having mechanically decoupled field generators to reduce ambient acoustic noise," U.S. patent US6043653 A, 2000.
- [9] W. A. Edelstein, R. P. Mallozzi, R. A. Hedeem, S. A. El-Hamamsy, M. L. Miller, and P. S. Thompson, "Low noise MRI scanner," U.S. patent US6437568 B1, 2002.
- [10] M. McJury, R. W. Stewart, D. Crawford, and E. Toma, "The use of active noise control (ANC) to reduce acoustic noise generated during MRI scanning: some initial results," *Magnetic Resonance Imaging*, vol. 15, no. 3, pp. 319–322, 1997.
- [11] P. Mansfield and B. Haywood, "Principles of active acoustic control in gradient coil design," *Magma: Magnetic Resonance Materials in Physics, Biology and Medicine*, vol. 10, no. 2, pp. 147–151, 2000.
- [12] P. Mansfield, B. Haywood, and R. Coxon, "Active acoustic control in gradient coils for MRI," *Magnetic Resonance in Medicine*, vol. 46, no. 4, pp. 807–818, 2001.
- [13] J. Chambers, D. Bullock, Y. Kahana, A. Kots, and A. Palmer, "Developments in active noise control sound systems for magnetic resonance imaging," *Applied Acoustics*, vol. 68, no. 3, pp. 281–295, 2007.
- [14] Y. Wang, F. Liu, X. Zhou, Y. Li, and S. Crozier, "A numerical study of the acoustic radiation due to eddy current-cryostat interactions," *Medical Physics*, vol. 44, no. 6, pp. 2196–2206, 2017.
- [15] F. Hennel, F. Girard, and T. Loenneker, "Silent MRI with soft gradient pulses," *Magnetic Resonance in Medicine*, vol. 42, no. 1, pp. 6–10, 1999.
- [16] F. Hennel, "Fast spin echo and fast gradient echo MRI with low acoustic noise," *Journal of Magnetic Resonance Imaging*, vol. 13, no. 6, pp. 960–966, 2001.
- [17] W. Shao and C. K. Mechefske, "Acoustic analysis of a gradient coil winding in an MRI scanner," *Concepts in Magnetic Resonance Part B: Magnetic Resonance Engineering*, vol. 24B, no. 1, pp. 15–27, 2005.
- [18] W. Shao and C. K. Mechefske, "Analysis of the sound field in finite length infinite baffled cylindrical ducts with vibrating walls of finite impedance," *Journal of the Acoustical Society of America*, vol. 117, no. 4, pp. 1728–1736, 2005.
- [19] L. K. Forbes, M. A. Brideson, S. Crozier, and P. T. While, "An analytical approach to the design of quiet cylindrical asymmetric gradient coils in MRI," *Concepts in Magnetic Resonance B*, vol. 37B, pp. 167–179, 2010.
- [20] F. Tang, J. Hao, F. Freschi et al., "A cone-shaped gradient coil design for high-resolution MRI head imaging," *Physics in Medicine and Biology*, vol. 64, no. 8, Article ID 085003, 2019.
- [21] C. K. Mechefske, G. Yao, W. Li, C. Gazdzinski, and B. K. Rutt, "Modal analysis and acoustic noise characterization of a 4T MRI gradient coil insert," *Concepts in Magnetic Resonance*, vol. 22B, no. 1, pp. 37–49, 2004.
- [22] M. Rausch, M. Gebhardt, M. Kaltenbacher, and H. Landes, "Computer-aided design of clinical magnetic resonance imaging scanners by coupled magnetomechanical-acoustic modeling," *IEEE Transactions on Magnetics*, vol. 41, no. 1, pp. 72–81, 2005.
- [23] G. Li and C. K. Mechefske, "Structural-acoustic modal analysis of cylindrical shells: application to MRI scanner systems," *Magnetic Resonance Materials in Physics, Biology and Medicine*, vol. 22, no. 6, pp. 353–364, 2009.
- [24] Y. Wang, F. Liu, and S. Crozier, "Simulation study of noise reduction methods for a split MRI system using a finite element method," *Medical Physics*, vol. 42, no. 12, pp. 7122–7131, 2015.
- [25] Y. Wang, F. Liu, E. Weber et al., "Acoustic analysis for a split MRI system using FE method," *Concepts in Magnetic Resonance Part B: Magnetic Resonance Engineering*, vol. 45, no. 2, pp. 85–96, 2015.
- [26] S. A. Winkler, A. Alejski, T. Wade, C. A. McKenzie, and B. K. Rutt, "On the accurate analysis of vibroacoustics in head insert gradient coils," *Magnetic Resonance in Medicine*, vol. 78, no. 4, pp. 1635–1645, 2017.
- [27] L. Kang, L. Xia, Q. Wang, Y. Wang, F. Tang, and F. Liu, "A volumetric finite-difference method for the design of three-dimensional, arbitrary-structured MRI gradient coil," *Review*

- of Scientific Instruments*, vol. 92, no. 3, Article ID 034712, 2021.
- [28] M. A. Brideson, L. K. Forbes, and S. Crozier, "Determining complicated winding patterns for shim coils using stream functions and the target-field method," *Concepts in Magnetic Resonance*, vol. 14, no. 1, pp. 9–18, 2002.
- [29] R. Aris, *Vectors, Tensors and the Basic Equations of Fluid Mechanics*, Dover, New York, NY, USA, 1962.
- [30] A. P. Boresi and K. P. Chong, *Elasticity in Engineering Mechanics*, Elsevier, New York, NY, USA, 1987.
- [31] M. Kamon, M. J. Tsuk, and J. K. White, "FASTHENRY: a multipole-accelerated 3-D inductance extraction program," *IEEE Transactions on Microwave Theory and Techniques*, vol. 42, no. 9, pp. 1750–1758, 1994.

RETRACTED